Published in: [Journal of Ambient Intelligence and Humanized Computing] journal.

The Version of Record is available online at: http://dx.doi.org/10.1007/s12652-021-02976-6

Adaptive trapezoid region intercept histogram based Otsu method for brain MR image segmentation

Leyi Xiao[1] · Chaodong Fan[1,2] · Honglin Ouyang[3] · Andrea F. Abate[4] · Shaohua Wan[5]

Abstract

In brain magnetic resonance (MR) image segmentation, the current Otsu method is often difficult to take both accuracy and anti-noise capability into consideration. So, in this paper, an adaptive trapezoid region intercept histogram based Otsu method is proposed. On the basis of bilateral filtering, the method uses Sigmoid function to identify the noise and adaptively calculate the weight of neighborhood pixel, and then constructs a 2D histogram of gray value-adaptive weight neighborhood gray mean to enhance the algorithm's anti-noise capability and detail retention. The hierarchical threshold model is adopted: the macro-threshold T_1 is determined by the trapezoid region intercept histogram based Otsu method, and the micro-threshold T_2 is determined by the between-class variance criterion again in the trapezoid region corresponding to T_1. The image is segmented by T_2 to improve the accuracy of image segmentation. Based on the neighborhood information, an adaptive parameter l is designed to identify and correct noise, thus enhancing the universality of the algorithm. The experimental results show that the proposed method is effective and can be well applied to MR image segmentation.

Keywords Image segmentation · Otsu method · Adaptive filtering · Hierarchical threshold · Brain MR image

1 Introduction

Brain diseases are gradually becoming a major disease that affects human health. The examination and analysis of brain tissue based on imaging technology is of great significance for the diagnosis and prevention of brain diseases (Song et al. 2014; Castiglione et al. 2017; Magudeeswaran and Bharath 2020). Among various imaging technologies, Magnetic resonance imaging (MRI) is widely used in the field of brain diagnosis because of its high resolution on soft tissues and its ability to distinguish each brain tissue more clearly (Castiglione et al. 2015; Adel et al. 2018; Krishnakumar and Manivannan 2020). Brain MR image segmentation based on MRI technology is a prerequisite for the diagnosis and analysis of the brain, and the segmentation effect has an important impact on the diagnosis result (Nie et al. 2018). Due to the large amount of data, the efficiency of manual segmentation is low and the segmentation effect is easily affected by personal subjective emotions. Therefore, how to quickly, accurately and automatically segment brain MR images is a current hotspot and difficulty in research (Bahar and Mehran 2018).

At present, various automatic image segmentation methods have appeared, which can be roughly divided into

✉ Shaohua Wan
shaohua.wan@ieee.org

Leyi Xiao
xiaolyttkx@163.com

Chaodong Fan
fchdmy@hnu.edu.cn

Honglin Ouyang
Oyhl1405.ouyang@vip.sina.com

Andrea F. Abate
abate@unisa.it

1 School of Information Technology and Management, Hunan University of Finance and Economics, Changsha 410205, China

2 Foshan Green Intelligent Manufacturing Research Institute of Xiangtan University, Foshan 528000, China

3 College of Electrical and Information Engineering, Hunan University, Changsha 410082, China

4 University of Salerno, Fisciano, Italy

5 School of Information and Safety Engineering, Zhongnan University of Economics and Law, Wuhan 430073, China

threshold segmentation (Bahar and Mehran 2018; Allioui et al. 2021), edge detection (Buvanesvari and Suganthi 2020), clustering segmentation (Zhao et al. 2019; Tongbram et al. 2021), regional growth (Javed et al. 2016), neural network method (Nie et al. 2018) and so on. Among these methods, although the neural network method has achieved good segmentation results, it needs to label many samples and the training process is time-consuming (Ding et al. 2020; Gao et al. 2020; Sankar and George 2020; Wan et al. 2020). So, threshold segmentation is still widely used in image segmentation because of its simplicity and effectiveness. Among them, the maximum between-class variance method (Otsu method) is a classical and effective method (Nobuyuki 1979). The 1D Otsu method only considers the gray information of the pixel but ignores its spatial correlation, so the algorithm's anti-noise capability is poor. In this regard, Liu et al. (1993) constructed a 2D histogram of gray value-neighborhood gray mean by introducing neighborhood gray mean, and thus proposed a 2D Otsu method with better anti-noise capability. In order to avoid the approximate calculation of 2D Otsu method, Zhang et al. (2011) proposed a precise 2D Otsu method (P2D_Otsu) by establishing an accurate threshold calculation formula. In order to enhance the algorithm's ability to deal with pepper and salt noise, Sha et al. (2016) adopted the median-mean gray of pixel instead of the traditional gray mean to construct a new 1D histogram, to enhance the algorithm's anti-noise universality. In order to avoid inaccurate segmentation caused by ignoring regions far from the diagonals in the 2D histogram cross partition method, Fan et al. (2007) proposed a 2D Otsu curve segmentation method by using a curve to partition the 2D histogram. Due to the variety of curves, it is difficult to quickly select the appropriate curve, so Wu et al. (2008) proposed the 2D oblique partition Otsu method by using a straight line perpendicular to the main diagonal to partition the 2D histogram. In order to improve the segmentation efficiency of 2D oblique partition Otsu method, He (2012) and Nie (2013) established a 1D Otsu criterion based on line intercept histogram. To further enhance the anti-noise capability of the algorithm, Li et al. (2017) reconstructed the 2D histogram after denoising, but the location of noise points depended on experience. In order to improve the efficiency and anti-noise capability of line intercept histogram based Otsu method, Xiao et al. (2019) proposed a trapezoid region intercept histogram based Otsu method, although this method shows good segmentation performance, the trapezoid side length r and parameter l are fixed by empirical values, so the algorithm's universality is not very well.

In order to enhance the universality of the trapezoid region intercept histogram based Otsu method to better segment different brain MR images, an adaptive trapezoid region intercept histogram based Otsu is proposed in this paper. In this method, the adaptive weighted neighborhood gray mean is used instead of the traditional neighborhood gray mean, and the 2D histogram of gray value-adaptive weighted neighborhood gray mean is established to separate the noise as much as possible. Giving the reasoning process of reasonable value of side length r, and the hierarchical threshold method is used to determine the accurate threshold. Adaptive parameter l is designed based on pixel neighborhood information to segment images with different noise. The segmentation experiments of brain MR images show that the proposed method has good anti-noise capability, timeliness and universality, and can segment brain MR images accurately.

Organization The rest of this paper is organized as follows: Sect. 2 introduces the trapezoid region intercept histogram based Otsu method, Sect. 3 elaborates the improvement methods of this paper, Sect. 4 tests and analyzes the performance of this method through the brain MR image segmentation experiment. Finally, conclusions are presented in Sect. 5.

2 Trapezoid region intercept histogram based Otsu method

In the 2D histogram of gray value-neighborhood gray mean shown in Fig. 1, the trapezoid region intercept histogram based Otsu method uses trapezoid with the base perpendicular to the main diagonal and side length r to partition the histogram into two parts: target and background. Suppose the gray value of the image is 0, 1, 2,…, $L-1$, (x_f, y_g) is a two-tuple

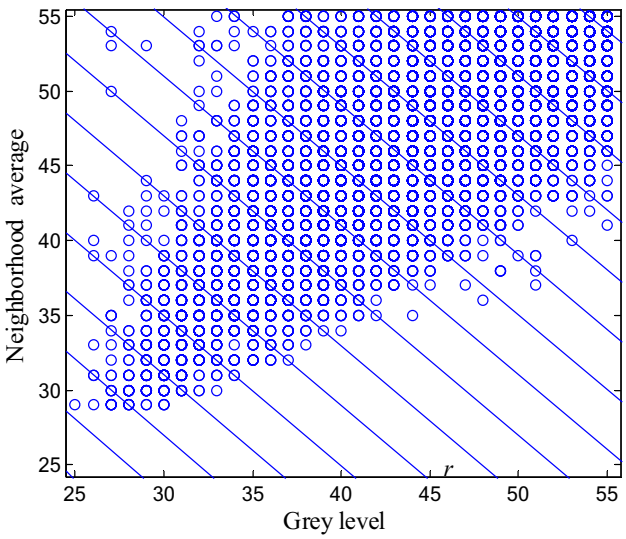

Fig. 1 The trapezoidal region partition 2D histogram

composed of the pixel's gray value and the neighborhood's gray mean. Image pixels are respectively mapped to trapezoidal regions with intercept 0, 1, 2,…,$round(2(L-1)/r)$ by $h_1(x_f, y_g) = round\big((x_f + y_g)/r\big)$ (where round (●) means to round off '●'). In order to correct the noise and enhance the anti-noise capability of the algorithm, Xiao et al. (2019) regarded the two regions of $|x_f - y_g| > l$ shown in Fig. 2 as noise regions (that is, the region where P_1 and P_2 are located), and the gray value is replaced by the neighborhood gray mean for noise correction. So, the above mapping can be modified as

$$h_2(x_f, y_g) = \begin{cases} round\big((x_f + y_g)/r\big), & |x_f - y_g| \le l \\ round\big((y_g + y_g)/r\big), & |x_f - y_g| > l \end{cases} \tag{1}$$

Suppose n_S is the number of all the pixels in the image that satisfy $h_2(x_f, y_g) = S$, then the frequency of the trapezoid region intercept S is:

$$p_S = \frac{n_S}{M \times N}, S = 0,1, \cdots, 2(L-1)/r \tag{2}$$

Based on the probability distribution of the trapezoid region intercept as shown in Eq. (2), the corresponding trapezoid region intercept histogram can be established. Based on the trapezoid region intercept histogram, the following maximum between-class variance criterion is given (Xiao et al. 2019):

$$\sigma_2^2(T) = \omega_0'(\mu_0' - \mu_T')^2 + \omega_1'(\mu_1' - \mu_T')^2 \tag{3}$$

where $\omega_0' = \sum_{S=0}^{T} p_S, \omega_1' = \sum_{S=T+1}^{2(L-1)/r} p_S, \mu_0' = \sum_{S=0}^{T}\left(S\frac{p_S}{\omega_0'}\right)\mu_1' = \sum_{S=T+1}^{2(L-1)/r}\left(S\frac{p_S}{\omega_1'}\right), \mu_T' = \sum_{S=0}^{2(L-1)/r} S p_S$.

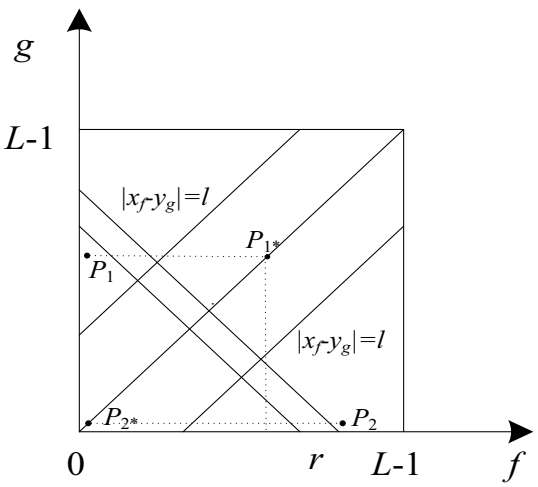

Fig. 2 Noise correction mechanism of trapezoid region intercept histogram based Otsu method

3 The proposed method

Although the above mentioned trapezoid region intercept histogram based Otsu method has good segmentation performance, it still has the following disadvantages: firstly, the neighborhood gray mean treats the pixels in the neighborhood equally, and does not fully consider the difference in position and gray of each pixel, so it cannot reflect the real situation of the current pixel. Secondly, although using trapezoid region to partition histogram can improve the efficiency of the algorithm, only the rough threshold is obtained and the segmentation is not accurate enough. Finally, without considering the actual situation of image and pixel, the parameter l is set as a fixed value, resulting in poor universality of the algorithm. In view of this, three corresponding improvement strategies are proposed to improve the segmentation performance of the trapezoid region intercept histogram based Otsu method.

3.1 2D histogram of gray value-adaptive weighted neighborhood gray mean

The trapezoid region intercept histogram based Otsu method is based on the 2D histogram of gray value-neighborhood gray mean, where the grayscale feature can keep the image information as much as possible, while the neighborhood gray mean feature can eliminate the noise as much as possible. Although mean filtering can effectively eliminate Gaussian noise, it fails to fully consider the actual situation of each pixel in the neighborhood, which is easily to cause image edge blurring. In this regard, Zhang et al. (2011) firstly sorted the pixels in the 8-decentroid neighborhood (that is, remove the center point in 8 neighborhood) according to their gray values, and then calculated the average gray value of the fourth and fifth after sorting, so as to obtain the new smooth image (We call this mean method the median-mean method). The median-mean method can effectively eliminate pepper and salt noise and keep the image details, but it is not effective in processing Gaussian noise. Tomasi et al. (1998) proposed the bilateral filtering, which considers the position between pixels and the correlation between gray values, can effectively eliminate Gaussian noise and maintain image details, and is a current filtering method with good performance. In view of the good performance of the bilateral filtering method, this paper uses it to replace the neighborhood gray mean of the pixel, and designs a 2D histogram of gray value-adaptive weighted neighborhood gray mean.

Suppose f is the original image, and η is its the smooth image after bilateral filtering. Suppose S_{xy} is the

neighborhood centered on pixel (x, y). $f(i, j)$, (i, j), $_s(i, j)$ and $_r(i, j)$ respectively represent the gray value, weight coefficient, spatial proximity factor and gray similarity factor at pixel (i, j) in S_{xy}. The expression of bilateral filtering is as follows:

$$\eta(x,y) = \frac{\sum_{(i,j)\in S_{xy}} \omega(i,j) f(i,j)}{\sum_{(i,j)\in S_{xy}} \omega(i,j)} \tag{4}$$

$$\omega(i,j) = \omega_s(i,j)\omega_r(i,j) \tag{5}$$

$$\omega_s(i,j) = e^{-\frac{|i-x|^2+|j-y|^2}{2\sigma_s^2}} \tag{6}$$

$$\omega_r(i,j) = e^{-\frac{|f(i,j)-f(x,y)|^2}{2\sigma_r^2}} \tag{7}$$

where σ_s and σ_r are the standard deviations of the Gaussian function, which control the attenuation degree of $_s(i, j)$ and $_r(i, j)$ respectively.

In order to analyze the filtering performance of the bilateral filtering method, the Slice 80 brain MR Image in the Medical Image Depository of Harvard University (Brain Web 2020) was taken as the object and $N_{Sxy} = 5 \times 5$ neighborhood as shown in Fig. 3a was selected for analysis (N_{Sxy} represents the size of neighborhood S_{xy}). Figure 3b is the gray value of each pixel in the neighborhood S_{xy}, Fig. 3c is the case that the current pixel is not a noise point but its neighborhood contains noise, and Fig. 3d is the case that the current pixel is a noise point. Assuming the parameters $\sigma_s = 1.5$ and $\sigma_r = 8$, the weight coefficients of Fig. 3c and d in the process of bilateral filtering are shown in Fig. 3e and f respectively.

According to Fig. 3e, when the center of the neighborhood is not a noise point, the method can calculate the weight of each neighborhood pixel well. However, as can be seen from Fig. 3f, if the center of the neighborhood is a noise point, the gray value of the pixel is significantly different from that of other normal pixels in the neighborhood. In this case, the weight of noise pixels in the neighborhood is relatively large, so it is difficult to effectively eliminate the noise. This is because the bilateral filtering method calculates the weight with the gray value of the neighborhood center as the target. So when the neighborhood center is a noise point, the target of filtering is to calculate the gray value of the center, which is based on the similar noise points in the neighborhood.

In view of the shortcomings of the bilateral filtering method, Ma et al. (2014) used the neighborhood median values instead of $f(x, y)$ in Eq. (7) to enhance the algorithm's anti-noise capability. However, when (x, y) is a normal pixel, this method will cause the loss of image information. In this paper, based on the difference between a pixel and other pixels in its neighborhood, Sigmoid function is used to identify whether the pixel is noise.

$$S(z) = \frac{1}{1+e^{-z}} \tag{8}$$

$$z(x,y) = -a + 2a \cdot \frac{\sum_{(i,j)\in S_{xy}} \frac{|f(i,j)-f(x,y)|}{\max\limits_{(i,j)\in S_{xy}} |f(i,j)-f(x,y)|+\varepsilon}}{N_{S_{xy}}} \tag{9}$$

where ε is the minimum value to prevent the denominator from being 0. Since the definition domain of Sigmoid function is a symmetric interval, the parameter a is introduced to make the range of $z \in [-a, a]$.

According to Eq. (9), when (x, y) is the noise point, its gray value is significantly different from that of other pixels in the neighborhood, so the closer $z(x, y)$ is to a. When $(x,$

(a) Slice80 brain MR image

92	86	86	90	72
98	90	84	90	70
110	98	86	88	70
106	102	94	86	70
98	100	100	90	76

(b) Gray value of each pixel in S_{xy}

92	86	86	90	72
255	90	84	90	70
110	98	86	88	70
106	102	94	255	70
98	255	100	90	76

(c) (x, y) is not a noise point, but its neighborhood contains noise

92	86	86	90	72
255	90	84	90	70
110	98	255	88	70
106	102	94	255	70
98	255	100	90	76

(d) (x, y) is the noise point

0.1276	0.3292	0.4111	0.2905	0.0366
4.0936e-98	0.5658	0.7761	0.5658	0.0446
0.0046	0.2600	1	0.7761	0.0556
0.0145	0.0868	0.4857	7.9732e-98	0.0446
0.0549	4.0936e-98	0.0889	0.2905	0.0774

(e) The weight coefficient of (c) is ω

1.2058e-91	4.0936e-98	5.1122e-98	1.3965e-93	4.0016e-115
0.3292	2.7201e-93	4.9085e-100	2.7201e-93	2.4807e-117
1.8954e-72	1.8675e-84	1	1.8975e-95	3.0980e-117
1.5528e-76	2.4098e-80	9.0254e-89	0.6412	2.4807e-117
3.9418e-85	0.3292	1.2558e-82	1.3965e-93	3.2748e-110

(f) The weight coefficient of (d) is ω

Fig. 3 Bilateral filtering process

y) is a normal pixel, its gray value is close to that of other pixels in the neighborhood, and the closer $z(x, y)$ is to $-a$. After the pixel is classified into noise and normal pixel by Sigmoid function, $f'(x, y)$ can be used to replace $f(x, y)$ in Eq. (7) to calculate the weight $w_r(i, j)$ according to whether the pixel is noise or not, where $f'(x, y)$ can be defined as:

$$f'(x,y) = (1 - S(z))f(x,y) + S(z)med\left(S_{xy}\right) \tag{10}$$

where med(S_{xy}) represents the gray median of neighborhood S_{xy}. According to Eq. (10), when S(z) is close to 1, (x, y) is a noise point, in this case, the median gray value of the neighborhood is used instead of $f(x, y)$ to enhance the algorithm's anti-noise capability. When S(z) is close to 0, (x, y) is a normal pixel point, at this time, $f(x, y)$ is still used to calculate the weight $w_r(i, j)$ to keep the image information, the bilateral filtering result obtained from this is denoted as $\eta'(x, y)$. Therefore, based on $f(x, y)$ and $\eta'(x, y)$, it is easily to establish a 2D histogram of gray value-adaptive weighted neighborhood gray mean, so that the algorithm can eliminate as many kinds of noises as possible while maintaining image details.

3.2 Calculation of hierarchical threshold and side length *r*

As can be seen from Fig. 4, the optimal threshold T_1 obtained by trapezoid region intercept histogram based Otsu method corresponds to a trapezoid region in the original 2D histogram. This method segmented the image based on the rough threshold T_1 without further classification of the pixels in the trapezoid region, so the segmentation was not accurate (Xiao et al. 2019). In this regard, this paper proposes a hierarchical threshold method, which firstly determines the macro-threshold T_1 based on Eq. (3), and then determines the micro-threshold T_2 based on the between-class variance criterion in the shaded trapezoid region as shown in Fig. 4, so as to further classify the pixels in the trapezoid region. Because the hierarchical threshold method can classify the pixels in trapezoid region, it is expected to improve the accuracy of image segmentation.

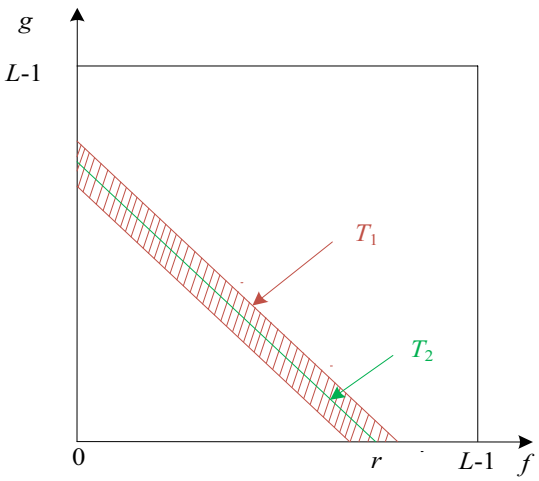

Fig. 4 Schematic diagram of the hierarchical threshold method

The value of r in trapezoid region intercept histogram based Otsu method is very important and has important influence on segmentation efficiency and quality. In this regard, the reasonable value of r was preliminarily analyzed through experiments (Xiao et al. 2019). In this section, the value of r was summarized and analyzed based on the hierarchical threshold structure. Assuming the threshold number is n, then $n \le \frac{L}{r}$ (L is the grayscale of the image, which is usually 256), so

1. When $n=1$, the calculation times of threshold T_1 at the macro level is $\frac{L}{r}$, the calculation times of threshold T_2 at the micro level is r, and the total calculation times is $\frac{L}{r} + r$. When $\frac{L}{r} = r$ (that is, $r = \sqrt{L} = 16$), the minimum number of calculations of the algorithm is $2\sqrt{L} = 32$.
2. When $n=2$, the calculation times of threshold at the macro level is $\left(\frac{L}{r}\right)^2$, the calculation times of threshold at the micro level is $2r$, and the total calculation times is $\left(\frac{L}{r}\right)^2 + 2r$. According to the generalization of the mean value inequality, $\left(\frac{L}{r}\right)^2 + 2r = \left(\frac{L}{r}\right)^2 + r + r \ge 3\sqrt[3]{\left(\frac{L}{r}\right)^2 rr}$. When $\left(\frac{L}{r}\right)^2 = r$ (that is, $r = \sqrt[3]{L^2} = 256^{\frac{2}{3}} = 32 \times 2^{\frac{1}{3}} \approx 40.317$), the minimum number of calculations of the algorithm is $3\sqrt[3]{L^2} \approx 121$.
3. When $n=3$, the calculation times of threshold at the macro level is $\left(\frac{L}{r}\right)^3$, the calculation times of threshold at the micro level is $3r$, and the total calculation times is $\left(\frac{L}{r}\right)^3 + 3r$. According to the generalization of the mean value inequality, $\left(\frac{L}{r}\right)^3 + 3r = \left(\frac{L}{r}\right)^3 + r + r + r \ge 4\sqrt[4]{\left(\frac{L}{r}\right)^3 rrr}$. When $\left(\frac{L}{r}\right)^3 = r$ (that is, $r = \sqrt[4]{L^3} = 64$), the minimum number of calculations of the algorithm is $4\sqrt[4]{L^3} = 256$.
4. When $n=4$, the calculation times of threshold at the macro level is $\left(\frac{L}{r}\right)^4$, the calculation times of threshold at the micro level is $4r$, and the total calculation times is $\left(\frac{L}{r}\right)^4 + 4r$. Similarly, we know that $\left(\frac{L}{r}\right)^4 + 4r \ge 5\sqrt[5]{\left(\frac{L}{r}\right)^4 rrrr}$. When $\left(\frac{L}{r}\right)^4 = r$ (that is, $r = \sqrt[5]{L^4} = 256^{\frac{4}{5}} \approx 84.449$), the minimum number of calculations of the algorithm is $5\sqrt[5]{L^4} \approx 422$. However, at this point, $\frac{L}{r} \approx 3 < n, (n = 4)$, so r cannot be 88.449, and r can only be $\frac{L}{n} = 64$ at most.

At this point, the total number of calculations is $\left(\frac{L}{r}\right)^4 + 4r = n^n + nr = n^n + L$.

5. According to the above analysis, when $n > 4$, r can only be $\frac{L}{n}$ at most. At this point, the calculation frequency of threshold value is n^n at the macro level, nr at the micro level, and $n^n + nr = n^n + L$ at the total.

3.3 Adaptive *l* based on neighborhood information

In order to effectively segment images with many kinds of noise, a 2D histogram of gray value-adaptive weight neighborhood gray mean is established in Sect. 3.1. This 2D histogram is composed of gray value and adaptive weighted neighborhood gray mean (where: the gray value should keep pixel information as much as possible, while the adaptive weighted neighborhood gray mean should restore the image as much as possible), so that the noise can be located as far away from the main diagonal as possible in the 2D histogram, and then the noise can be identified and filtered later based on parameter l. However, as shown in Fig. 2, according to the relationship between $|x_f - y_g|$ and l, the noise is recognized by the trapezoid region intercept histogram based Otsu method, and the recognition effect is heavily dependent on the parameter l. However, the reasonable value of l depends on the situation of the image itself, and it is usually impossible to determine its uniform value in advance. In this regard, we took Slice100 brain MR images as the objects to analyze the noise recognition when $l = 10$, 40, 70, 100 and 130, which the pepper and salt noise intensity λ in these images is 0.001, 0.05 and 0.1, respectively. As can be seen from Fig. 5, when $l = 10$, this method can better identify the noise in the image, but some normal pixels are mistaken for noise. When $l = 100$ or 130, this method will not mistake normal pixel for noise, but there are still a lot of noise in the image that are not recognized normally. It can be seen that when l is small, normal pixels may be mistaken for noise. When l is larger, a large number of noise cannot be recognized normally. Therefore, when $\lambda = 0.001$, the noise interference is small, then l is suitable to take a larger value (such as $l = 100$ or 130). When $\lambda = 0.1$, the noise interference is large, and l is suitable to take a smaller value (such as $l = 40$). When $\lambda = 0.05$, the noise interference is moderate, and the value of l should be neither too large nor too small (such as $l = 40$ or 70). In addition, by comparing the recognition effects of different l values on the same image, we find that different noise points can be identified based on different l values. Therefore, for images with different noise or different pixels in the same image, the ideal value

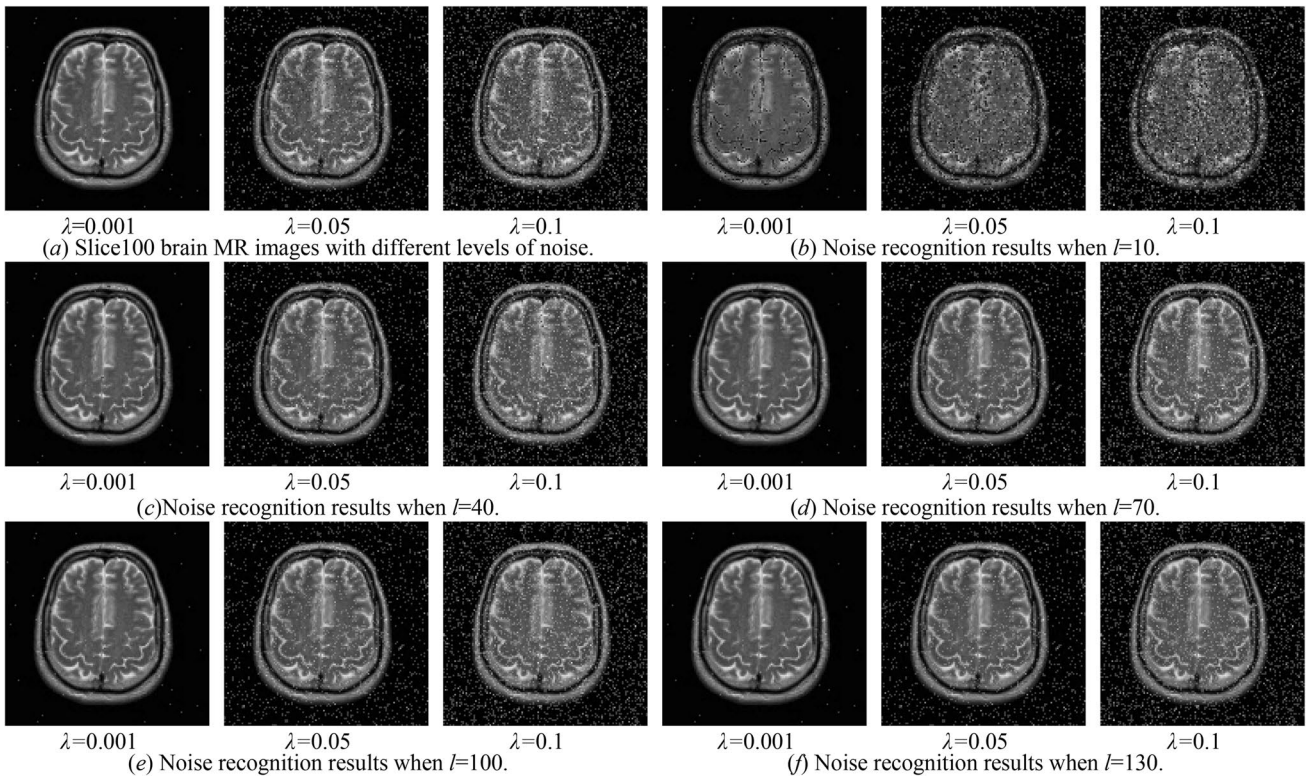

Fig. 5 Effect analysis of parameter l on noise recognition

of l varies, so the method of specifying the uniform value of l in advance is not universal.

In order to distinguish the image with different noise and each pixel in the image, we use the recognition result of Eq. (8) to design an adaptive method of parameter l.

$$l_{ij} = l_{min} + \beta(l_{max} - l_{min})(1 - S(z)) \tag{11}$$

where l_{ij} is the l value of pixel (i, j), S(z) is the noise recognition result of pixel (i, j) based on Eq. (8), β is the regulator to prevent l_{ij} from getting too large, and l_{min} and l_{max} are the minimum and maximum values of $|x_f\text{-}y_g|$ of all pixels in the current image.

As can be seen from above, this paper adopts the improved bilateral filtering result η' instead of the traditional mean filtering y_g for image segmentation. Therefore, y_g and l in Eq. (1) are replaced by η' and l_{ij} respectively, then Eq. (1) can be modified as:

$$h_2^*(x_f, \eta') = \begin{cases} round\big((x_f + \eta')/r\big), & |x_f - \eta'| \le l_{ij} \\ round\big((\eta' + \eta')/r\big), & |x_f - \eta'| > l_{ij} \end{cases} \tag{12}$$

According to Eq. (12), the larger S(z) is, the more likely the pixel (i, j) is to be a noise point, and the closer the l_{ij} is to l_{min}, so that $|x_f - \eta'| > l_{ij}$ is established to judge the pixel as a noise point. The smaller S(z) is, the more likely it is that the pixel (i, j) is to be a normal pixel, and the closer l_{ij} is to l_{max}, so that $|x_f - \eta'| \le l_{ij}$ is established to judge that the pixel is not a noise point. It can be seen that Eq. (11) can be used to calculate the value of the parameter l according to the actual situation of the pixel itself, while Eq. (12) can identify and correct the noise according to the calculation result of Eq. (11), so as to enhance the anti-noise capability of the algorithm.

3.4 Implementation of the adaptive trapezoid region intercept histogram based Otsu method

The specific implementation steps of the adaptive trapezoid region intercept histogram based Otsu method are as follows:

Step1 Input image f, initialization parameters $\sigma_s = 1.5$, $\sigma_r = 8$, $a = 10$, $l_{min} = 0$, $l_{max} = \frac{L-1}{\sqrt{2}}$.

Step2 According to Eq. (10), the intermediate quantity f' is calculated and $f(x,y)$ in Eq. (7) is replaced by $f'(x,y)$, so as to obtain the adaptive weight neighborhood gray mean based on bilateral filtering, and establish a 2D histogram of gray value-adaptive weight neighborhood gray mean.

Step3 According to Eq. (11), the adaptive parameter l_{ij} of pixel (i,j) is calculated, and adaptive filtering is performed according to Eq. (12).

Step4 According to the method in Sect. 3.2, the side length r was determined, and the trapezoid region intercept histogram was established, and the macro-threshold T_1 was solved by the maximum between-class variance criterion.

Step5 In the trapezoid region corresponding to the macro-threshold T_1, the maximum between-class variance criterion is used to calculate the micro-threshold T_2.

Step6 Segment the image according to the micro-threshold T_2 to obtain the segmentation result.

Step7 Output the result image after segmentation.

4 Test experiment and result analysis

4.1 Experimental setting and image data set

In order to test the segmentation performance of adaptive trapezoid region intercept histogram based Otsu method, this paper selected brain MR images from Slice 16–105 in the Medical Image Depository of Harvard University (Brain Web 2020) as objects and conducted the following two groups of experiments respectively: (1) effectiveness verification experiments of algorithm improvement. The adaptive weighted neighborhood mean filter in Sect. 3.1, mean filter, median filter and bilateral filter were used to denoising the brain MR images with different noises to verify the performance of the adaptive weighted neighborhood mean filter, so as to analyze the rationality of constructing a 2D histogram based on the adaptive weighted neighborhood gray mean. On the basis of the trapezoid region intercept histogram based Otsu method, the hierarchical threshold method is introduced to reclassify the trapezoid domain to improve the accuracy of image segmentation, so as to analyze the effectiveness of the hierarchical threshold method to improve the algorithm. In order to analyze the influence of adaptive l on the algorithm's anti-noise capability, the trapezoid region intercept histogram based Otsu methods using adaptive l and fixed l were compared. (2) Segmentation performance test experiments. In order to analyze the anti-noise capability, timeliness and detail retention of the adaptive trapezoid region intercept histogram based Otsu method, a single threshold segmentation experiment was carried out comparing with several current mainstream Otsu methods. Compared qualitatively and quantitatively with the multi-level thresholding segmentation methods of brain MR image, which have good performance at present, so as to analyze the applicability of the adaptive trapezoid region intercept histogram based Otsu method to brain MR image segmentation. All experiments were implemented by Matlab (R2011a). The parameter ε was set as the default minimum value of 2.2204×10^{-16} in Matlab, and the parameter $a = 10$. The CPU of the PC was Intel (R) Celeron(R) 1.50 GHz and RAM was 2.0 GB.

4.2 Effectiveness test of this improved method

4.2.1 Performance test of adaptive weighted neighborhood mean filtering

To verify the effectiveness of the adaptive weighted neighborhood mean filtering method, Slice 16–105 brain MR images were divided into five groups: slice 16–33, slice 34–51, slice 52–69, slice 70–87, and slice 88–105. Slice 16–33 brain MR images contain pepper and salt noise with density $\lambda = 0.05$; Slice 34–51 brain MR images contain Gaussian noise with mean $m = 0$ and variance $var = 0.03$; slice 52–69 brain MR images contain Gauss-pepper and salt mixed noise (pepper and salt noise with density $\lambda = 0.05$, Gaussian noise mean with $m = 0$ and variance $var = 0.03$); slice 70–87 brain MR images contain Poisson noise; slice 88–105 brain MR images contain Speckle noise with variance $var = 0.04$. Slice 16–105 brain MR images were filtered by adaptive weighted neighborhood mean filter, mean filter, median filter and bilateral filter, etc. Figure 6 shows some images and their filtering results.

It can be seen from Fig. 6 that the mean filtering method can eliminate Gaussian noise well, but it has poor processing effect on pepper and salt noise. The median filter method can eliminate the pepper and salt noise well, but it has poor effect on Gaussian noise and Speckle noise. The filtering effect of the bilateral filtering method is close to that of the mean filtering method, but it can keep the edge details of the image better and the processing effect of Speckle noise is relatively good. Based on the bilateral filtering method, the adaptive weighted neighborhood mean filtering method can calculate weight adaptively according to whether the current pixel is noise or not, so it can keep the image details well and achieve relatively good filtering effect for all kinds of noises. It can be seen that the adaptive weighted neighborhood mean filtering method can recover the image better, and the 2D histogram constructed based on this method can better distribute the noise in the region far away from the diagonal, thus providing good conditions for the subsequent noise correction.

4.2.2 Performance test of hierarchical threshold method

In order to verify the effectiveness of the hierarchical threshold method, which was used to improve the trapezoid region intercept histogram based Otsu method, and the experimental results were compared and analyzed with the traditional trapezoid region intercept histogram based Otsu method. In order to make the comparison clearer and distinguish the segmentation effects of the two methods from the visual perspective, $l = 20$, 30, and 40 were used to segment slice 16–51, slice 52–87, and slice 88–105 brain MR images, respectively. Figure 7 shows the segmentation results of partial images. It can be seen from Fig. 7 that although the difference between the two is small, it can still be found that the trapezoid region intercept histogram based Otsu method based on the hierarchical threshold can better preserve the image details. It can be seen that the hierarchical threshold method can improve the accuracy of image segmentation to some extent because it can reclassify the pixels in the trapezoid region. Therefore, the rationality and effectiveness of the hierarchical threshold method adopted in this paper are verified experimentally.

4.2.3 Performance test of adaptive *l*

In order to analyze the influence of adaptive parameter l on the algorithm's anti-noise capability, slice 16–105 brain MR images were divided into five groups as in Sect. 4.2.1: slice 16–33, slice 34–51, slice 52–69, slice 70–87, and slice 88–105. Pepper and salt noise with density $\lambda = 0.02$, 0.04, 0.06, 0.08 and 0.1 was added to these five groups of images to better distinguish the experimental results from the visual perspective. In the experiment, the trapezoid region intercept histogram based Otsu methods at $l = 10$, 40, 70, 100 and 130 were used to segment the above five groups of images, and the experimental results were compared with the segmentation results of the trapezoid region intercept histogram based Otsu method with adaptive parameter l. Figure 8 shows the segmentation results of some images. It can be seen from Fig. 8 that the trapezoid region intercept histogram based Otsu method can identify and correct most of the noise in the images when $l = 10$ and 40, but the loss of image detail information is caused by a large number of misrecognition. Although the algorithm can keep the image details well when $l = 100$ and 130, a large number of noises are not recognized. When adaptive l is adopted, the algorithm can remove the noise well while keeping the image details. In short, the smaller l, the more complete the noise recognition, but the higher the error recognition rate, the more serious the detail loss. The larger the l, the better the detail retention, but the less noise is identified. Therefore, when the noise interference is small, the main consideration should be to keep the image details, so it is appropriate to take a large value of l; when the noise interference is large, the noise factor should be mainly considered, and it is appropriate to take a small value of l. However, as the image is often unpredictable due to noise interference, and different pixels in the same image are interfered by noise differently, it is difficult to specify a uniform value of l in advance in practical application. Adaptive l can adaptively calculate the l value according to the difference between the current pixel and the surrounding pixel, so every pixel has the corresponding l value (instead of using the same l value for all the pixels of

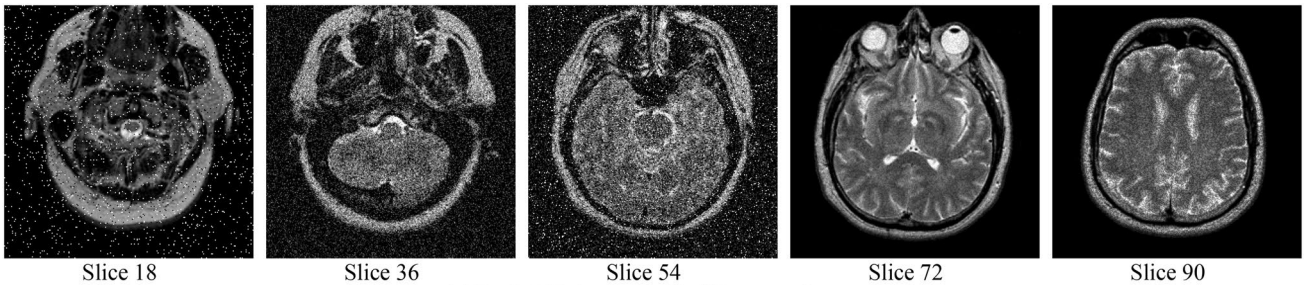

(*a*) Brain MR images with different noises.

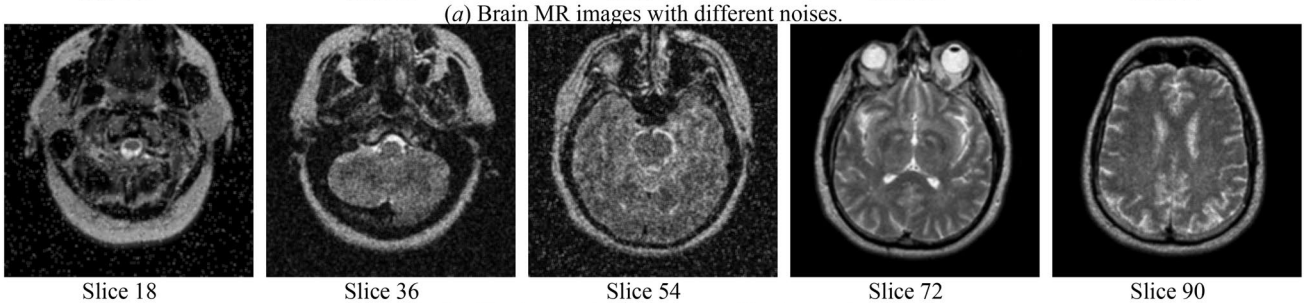

(*b*) The filtering results of the mean filtering method.

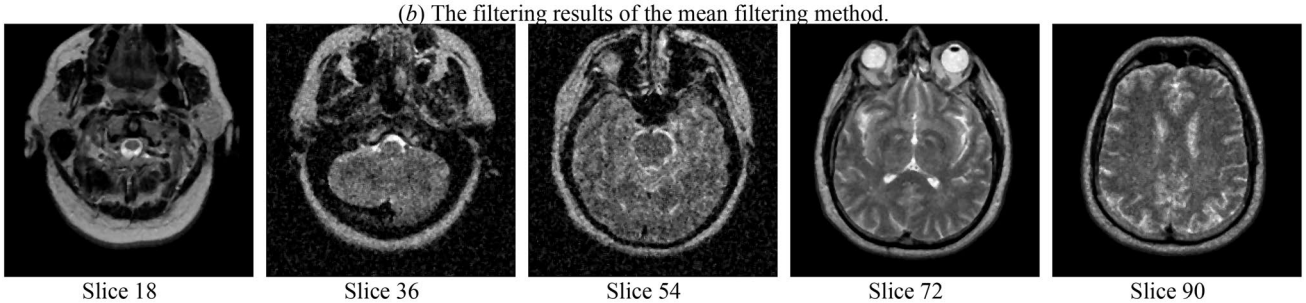

(*c*) The filtering results of the median filtering method.

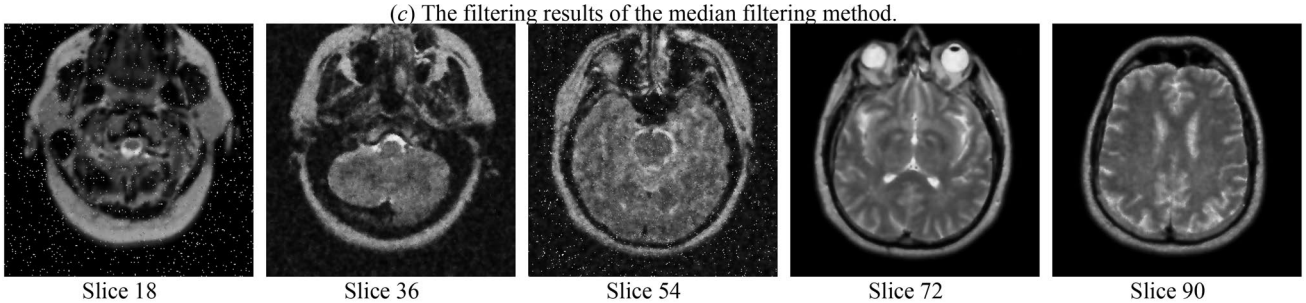

(*d*) The filtering result of bilateral filtering method.

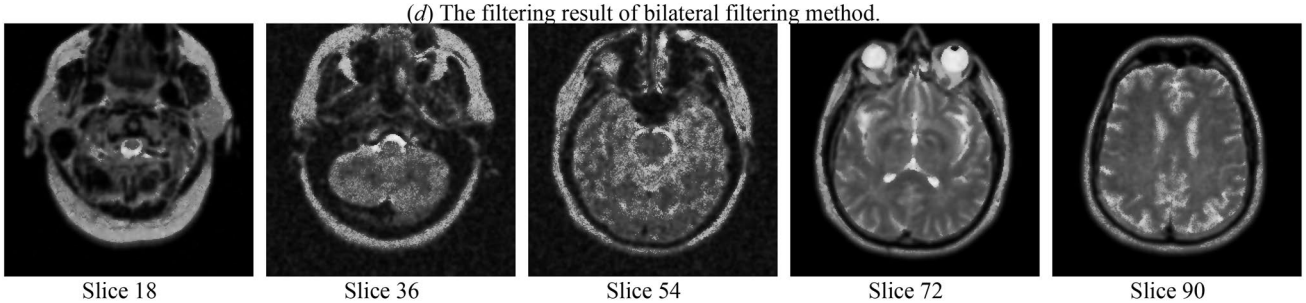

(*e*) Filtering results of adaptive weighted neighborhood mean method.

Fig. 6 Comparison of filtering effects of different filtering methods

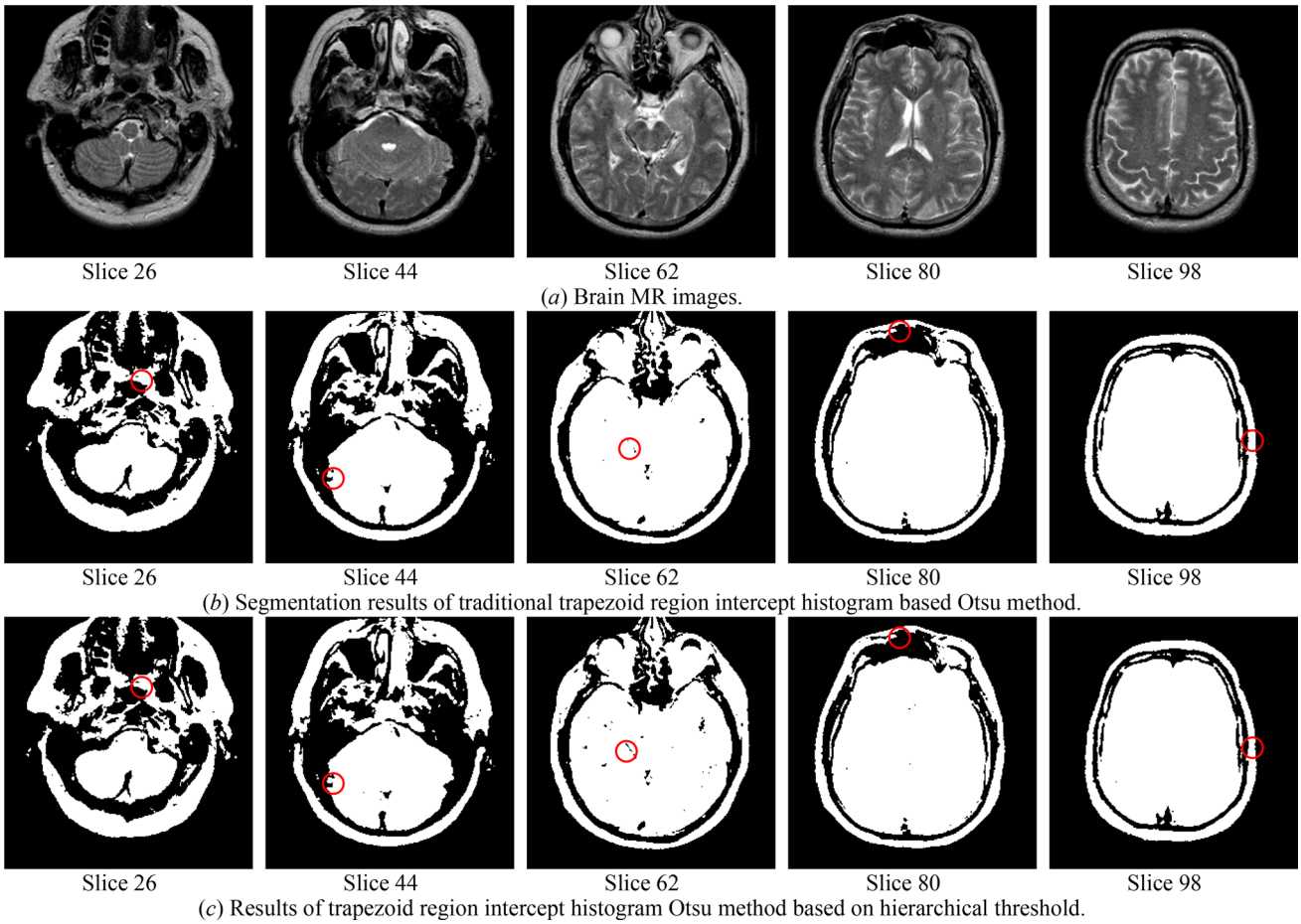

Fig. 7 Comparison of the segmentation effect of the trapezoid region intercept histogram based Otsu method with and without the hierarchical threshold method

the whole image), so it can process each pixel in the image differently. This method does not need the prior knowledge of image, so it has stronger universality and practicability.

4.3 Comparison of segmentation performance

In order to further test the algorithm's segmentation performance, this paper selects four measurements (Xiao et al. 2019), namely Peak Signal to Noise Ratio (PSNR), Misclassification Error (ME), Structural Similarity Index (SSIM) and Root Mean Squared Error (RMSE), to conduct quantitative analysis on the performance of this algorithm. The quantitative comparison experiment in this section includes the following two parts: (1) in order to analyze the segmentation performance of adaptive trapezoid region intercept histogram based Otsu method, it is firstly compared with several improved Otsu methods with good performance. Since some improved Otsu methods are difficult to extend to multiple thresholds, for the convenience of comparison, all the algorithms use single threshold to segment image. (2) In view of the complexity of brain MR images, multi-level thresholding segmentation is usually required, so it is quantitative comparison with several current multi-level thresholding segmentation methods to verify the applicability of this method to brain MR image segmentation.

4.3.1 Comparative analysis with other Otsu methods

To verify the effectiveness of adaptive trapezoid region intercept histogram based Otsu method (ATRIH_Otsu), it is compared with several improved 2D histogram Otsu methods such as Median filtered Otsu method (Median_Otsu), mean filtered Otsu method (Mean_Otsu),

Precise 2D Otsu method (P2D_Otsu) (Zhang et al. 2011), Robust 2D Otsu method (R2d_Otsu) (Sha et al. 2016), Adaptive angle threshold based Otsu method (AAT_Otsu) (Xiao et al. 2020) and Trapezoid region intercept histogram based Otsu method (TRIH_Otsu) (Xiao et al. 2019). To make the comparison more obvious, the slice 16–105 brain MR images with noise in Fig. 7a were used as the test objects, and the neighborhood size of all methods was 5×5. Because ATRIH_ Otsu was found to be able to take into account all

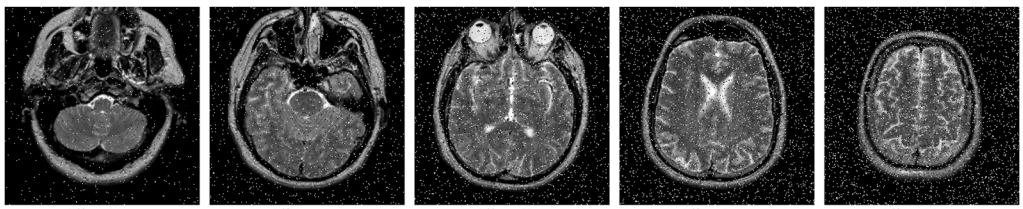

(*a*) Brain MR images with different levels of noise.

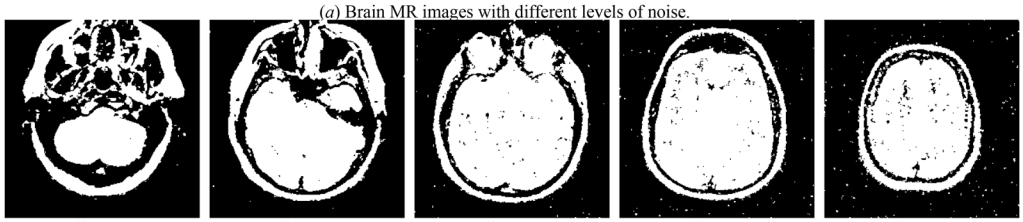

(*b*) Segmentation results by trapezoid region intercept histogram based Otsu method when *l*=10.

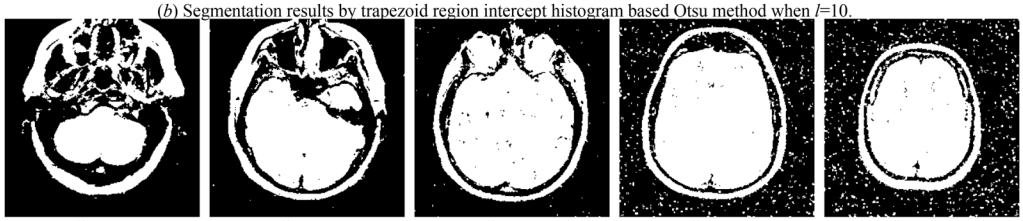

(*c*) Segmentation results by trapezoid region intercept histogram based Otsu method when *l*=40.

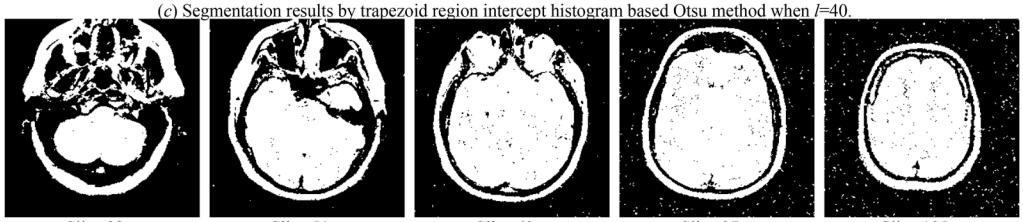

(*d*) Segmentation results by trapezoid region intercept histogram based Otsu method when *l*=70.

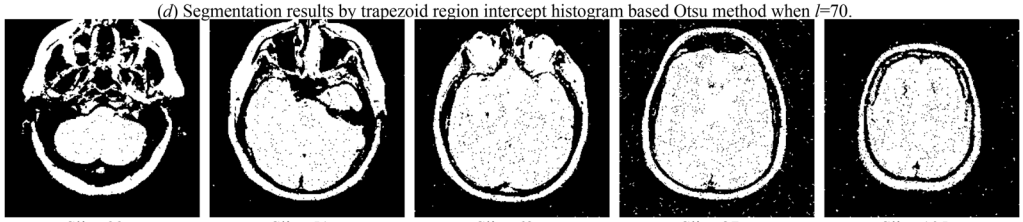

(*e*) Segmentation results by trapezoid region intercept histogram based Otsu method when *l*=100.

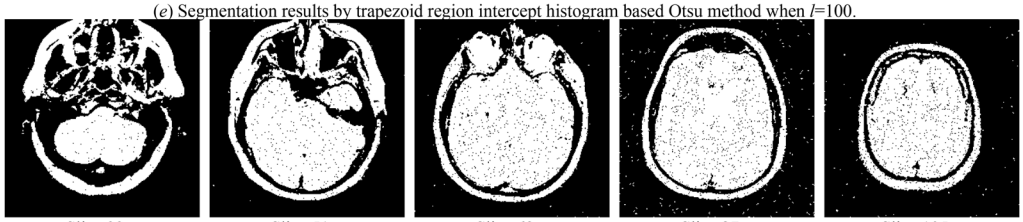

(*f*) Segmentation results by trapezoid region intercept histogram based Otsu method when *l*=130.

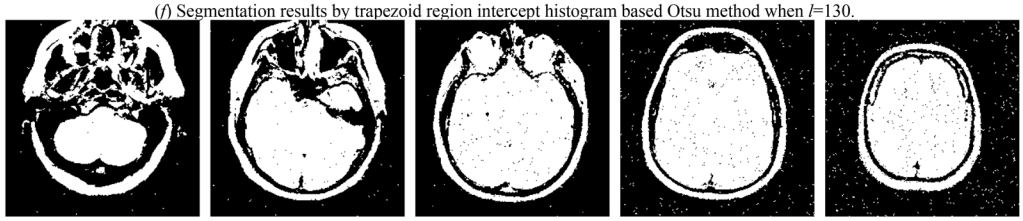

(*g*) Segmentation results by adaptive *l* trapezoidal region intercept histogram based Otsu method.

Fig. 8 Comparison of segmentation effect of fixed and adaptive *l* by trapezoid region intercept histogram based Otsu method

Table 1 PSNR values of each improved 2D Otsu method

Method	Sclice18	Sclice36	Sclice54	Sclice72	Sclice90
P2D_Otsu	7.4123	9.1263	10.9294	13.2892	14.4210
R2D_Otsu	11.0023	11.0518	12.6296	14.2572	17.0220
AAT_Otsu	12.5921	12.2165	11.5990	15.6484	19.1611
TRIH_Otsu	12.8743	12.3761	12.7043	15.7718	18.7348
Median_Otsu	17.1853	12.9195	12.3408	18.4381	20.6397
Mean_Otsu	13.9062	13.1845	11.5391	17.2306	20.6213
ATRIH_Otsu	15.4814	13.5799	12.8220	17.2096	20.6520

Table 2 ME values of each improved 2D Otsu method

Method	Sclice18	Sclice36	Sclice54	Sclice72	Sclice90
P2D_Otsu	0.2220	0.1828	0.1402	0.0859	0.0671
R2D_Otsu	0.1272	0.1287	0.0998	0.0702	0.0384
AAT_Otsu	0.0980	0.1130	0.1273	0.0533	0.0241
TRIH_Otsu	0.0935	0.1036	0.0994	0.0508	0.0264
Median_Otsu	0.0377	0.0973	0.1099	0.0284	0.0179
Mean_Otsu	0.0773	0.0921	0.1304	0.0352	0.0183
ATRIH_Otsu	0.0526	0.0839	0.0993	0.0372	0.0172

Table 3 SSIM values of each improved 2D Otsu method

Method	Sclice18	Sclice36	Sclice54	Sclice72	Sclice90
P2D_Otsu	0.6056	0.7329	0.8390	0.9066	0.9270
R2D_Otsu	0.8127	0.8245	0.8906	0.9251	0.9598
AAT_Otsu	0.8658	0.8542	0.8579	0.9454	0.9754
TRIH_Otsu	0.8685	0.8701	0.8923	0.9471	0.9729
Median_Otsu	0.9541	0.8831	0.8814	0.9713	0.9801
Mean_Otsu	0.9031	0.8882	0.8571	0.9622	0.9747
ATRIH_Otsu	0.9322	0.9005	0.8941	0.9620	0.9826

Table 4 RMSE values of each improved 2D Otsu method

Method	Sclice18	Sclice36	Sclice54	Sclice72	Sclice90
P2D_Otsu	108.6245	89.1713	72.4551	55.2181	48.4720
R2D_Otsu	71.8501	71.4415	59.5744	49.3946	35.9285
AAT_Otsu	59.8320	62.4766	67.0794	42.0842	28.0856
TRIH_Otsu	57.9192	61.3387	59.0642	41.4906	29.4985
Median_Otsu	35.2595	57.6187	61.5889	30.5234	23.6949
Mean_Otsu	51.4316	55.8879	67.5437	35.0761	23.7397
ATRIH_Otsu	42.9015	53.4003	58.2694	35.1608	23.6559

kinds of noises when $\beta = 0.2$, so $\beta = 0.2$ was used in this paper.

Tables 1, 2, 3 and 4 show the quantitative comparison results of the images in Fig. 6a. From Tables 1, 2, 3, and 4, it can be seen that PSNR and SSIM of P2D_Otsu are relatively minimum (ME and RMSE are relatively maximum), which is due to the inaccuracy of image segmentation caused by the cross partition of 2D histogram in this method. Compared with P2D_Otsu, R2d_Otsu uses post-processing operation to correct the noise, so its PSNR and SSIM are larger (ME and RMSE are smaller). Because the noise correction strategy of AAT_Otsu, TRIH_Otsu and ATRIH_Otsu only corrects part of the noise, which avoids the loss of image information to a certain extent, their segmentation effect is relatively better. Except Slice 90, the PSNR and SSIM (ME and RMSE) of TRIH_Otsu and ATRIH_Otsu are respectively larger (smaller) than those of AAT_Otsu, indicating that it is more reasonable to partition 2D histogram by trapezoids perpendicular to the main diagonal than by angle. Mean filtering can remove Gaussian noise well, but it is easy to smooth the image, so PSNR and SSIM (ME and RMSE) are bigger (smaller) than Median_Otsu when it is used to segment images with Gaussian noise. It can be seen that if the type and intensity of noise contained in the image are known in advance, the method of filtering first and then segmentation has better segmentation. However, the noise in the actual application of the image is often unpredictable, blind filtering may lose the image information. On the whole, ATRIH_Otsu's PSNR and SSIM are relatively maximum (ME and RMSE are relatively minimum), indicating that this method has relatively good segmentation performance for all kinds of noises. This comparative experiment verifies the effectiveness of the three improvement strategies from a quantitative perspective.

Table 5 Segmentation Efficiency of each improved 2-D Otsu method (/ms)

Method	Sclice18	Sclice36	Sclice54	Sclice72	Sclice90
P2D_Otsu	52.578	52.761	52.586	52.635	52.331
R2D_Otsu	30.253	30.373	30.417	30.046	29.905
AAT_Otsu	9.695	9.586	9.594	9.452	9.654
TRIH_Otsu	3.476	3.767	3.563	3.639	3.645
Median_Otsu	9.911	9.817	9.948	9.653	9.850
Mean_Otsu	9.851	10.099	9.811	9.677	9.703
ATRIH_Otsu	7.418	7.589	7.575	7.370	7.675

In terms of algorithm efficiency, assume that the image gray scale ranges from 0 to L, AAT_Otsu's angle threshold range from 0 to θ. The complexity of P2D_Otsu's algorithm is $O(L^2)$, the complexity of R2D_Otsu, Median_Otsu, Mean_Otsu, AAT_Otsu and TRIH_Otsu is $O(2L)$, $O(L)$, $O(L)$, $O(\theta)$ and $O(L/r)$ respectively. The ATRIH_Otsu uses a hierarchical threshold model, where the value of macro-threshold T_1 ranges from 0 to L/r and the value of micro-threshold T_2 ranges from T_1 to (T_1+r), so this algorithm's complexity is $O(L/r+r)$. Table 5 shows that in terms of algorithm efficiency, the performance of each algorithm is ranked as:

TRIH_Otsu > ATRIH_Otsu > AAT_Otsu > Median_Otsu ≈ Mean_Otsu > R2D_Otsu > P2D_Otsu

4.3.2 Comparison with other multi-level thresholding segmentation methods for brain MR image

Due to the complexity of brain tissues, multiple thresholds are often needed to separate different brain tissues. Therefore, in this section, Slice 20, Slice 40, Slice 60 and Slice 80 brain MR images with different noises (Xiao et al. 2019) were selected for this multi-level thresholding segmentation experiment. As shown in Fig. 9, the four images contain pepper and salt noise, Gaussian noise, Poisson noise and Speckle noise, respectively. To verify the multi-level thresholding segmentation performance of ATRIH_Otsu, it was compared with the Efficient cuckoo search based Otsu method (ECS_Otsu) (Shilpa and Shyam 2016), Evolutionary gray gradient based Otsu method (EGG_Otsu) (Rutuparna et al. 2017), Non-local means 2D histogram based Renyi entropy method (NLM2D_ Renyi) (Himanshu and Mukesh 2018) and Trapezoid region intercept histogram based Otsu method, TRIH_Otsu) (Xiao et al. 2019), which are currently good multi-level thresholding segmentation methods. Among them, ECS_Otsu is based on 1D gray histogram, while other methods are based on improved 2D histogram. For convenience of comparison, this paper only compares the segmentation performance of various methods based on RMSE, SSIM, PSNR and ME, as in literature (Xiao et al. 2019).

Tables 6, 7, 8 and 9 respectively show RMSE, SSIM, PSNR and ME of various algorithms when the threshold number $m = 2, 3, 4, 5$, among which the experimental data of ECS_Otsu, EGG_Otsu, NLM2D_Renyi and TRIH_Otsu are from literature (Xiao et al. 2019). From the comparison results, we can see that the RMSE and ME (SSIM and PSNR) of ECS_Otsu are relatively maximum (minimum), indicating that the 2D gray histogram has an obvious advantage over the traditional 1D gray histogram in noise resistance. TRIH_Otsu and ATRIH_Otsu both corrected the noise to some extent, so SSIM and PSNR (RMSE and ME) of them were relatively larger (smaller) than EGG_Otsu and NLM2D_Renyi. ATRIH_Otsu not only uses the hierarchical threshold method to improve the accuracy of image segmentation, but also can adaptively identify and correct noise according to the specific situation of the image, so its SSIM and PSNR(RMSE and ME) are relatively maximum (minimum). In addition, we can also see that RMSE (SSIM and PSNR) of each method shows a trend of gradually decreasing (increasing) with the increase of threshold number, indicating that the segmentation quality of each method is

Table 6 Comparison of slice 20 brain image segmentation performance by different methods

Algorithms	m	RMSE	SSIM	PSNR	ME
ECS_Otsu	2	33.3541	0.7014	17.6678	0.0531
	3	32.5233	0.7862	17.8869	0.0680
	4	32.3402	0.7959	17.9359	0.0810
	5	30.7660	0.8164	18.3694	0.0980
EGG_Otsu	2	30.4784	0.7466	18.4510	0.0439
	3	28.6134	0.8038	18.9994	0.0621
	4	28.2897	0.8247	19.0982	0.0801
	5	28.2590	0.8327	19.1077	0.0868
NLM2D_Rényi	2	32.0194	0.7465	18.0225	0.0446
	3	29.0551	0.7947	18.8664	0.0626
	4	28.5015	0.8206	19.0334	0.0806
	5	28.3872	0.8312	19.0684	0.0965
TRIH_Otsu	2	25.2448	0.8177	20.0874	0.0258
	3	21.1759	0.8871	21.6140	0.0320
	4	17.7868	0.9242	23.1289	0.0328
	5	15.7361	0.9442	24.1928	0.0335
ATRIH_Otsu	2	15.4491	0.9503	24.3527	0.0121
	3	12.0960	0.9701	26.4779	0.0123
	4	10.2211	0.9787	27.9409	0.0131
	5	9.1337	0.9830	28.9178	0.0144

(a) Slice20 (b) Slice40 (c) Slice60 (d) Slice80

Fig. 9 Brain MR images with different noises

Table 7 Comparison of slice 40 brain image segmentation performance by different methods

Algorithms	m	RMSE	SSIM	PSNR	ME
ECS_Otsu	2	36.6692	0.7229	16.8448	0.0561
	3	28.1544	0.8481	19.1399	0.0642
	4	23.9766	0.8959	20.5351	0.0644
	5	22.6010	0.9108	21.0483	0.0731
EGG_Otsu	2	30.4218	0.8131	18.4671	0.0430
	3	26.0676	0.8787	19.8088	0.0543
	4	25.1190	0.8980	20.1308	0.0711
	5	22.0542	0.9173	21.2610	0.0724
NLM2D_Rényi	2	29.2365	0.8225	18.8123	0.0408
	3	25.3724	0.8808	20.0436	0.0518
	4	23.0701	0.9059	20.8698	0.0600
	5	21.1109	0.9273	21.6407	0.0646
TRIH_Otsu	2	25.0104	0.8648	20.1684	0.0242
	3	20.8863	0.9176	21.7336	0.0315
	4	18.3760	0.9394	22.8458	0.0320
	5	16.8840	0.9505	23.5813	0.0332
ATRIH_Otsu	2	21.4065	0.9200	21.5199	0.0215
	3	18.7783	0.9379	22.6577	0.0226
	4	17.8861	0.9438	23.0805	0.0263
	5	16.6521	0.9508	23.7014	0.0264

Table 8 Comparison of slice 60 brain image segmentation performance by different methods

Algorithms	M	RMSE	SSIM	PSNR	ME
ECS_Otsu	2	41.7006	0.6821	15.7280	0.0238
	3	28.3779	0.8634	19.0712	0.0264
	4	22.9264	0.9074	20.9241	0.0527
	5	20.1931	0.9301	22.0268	0.0678
EGG_Otsu	2	34.0555	0.7729	17.4871	0.0198
	3	27.1168	0.8649	19.4660	0.0271
	4	20.5753	0.9264	21.8639	0.0316
	5	17.3279	0.9480	23.3559	0.0348
NLM2D_Rényi	2	32.0218	0.7965	18.0219	0.0196
	3	25.3200	0.8810	20.0615	0.0206
	4	20.3917	0.9298	21.9417	0.0211
	5	16.1593	0.9554	23.9624	0.0215
TRIH_Otsu	2	30.9271	0.8136	18.3240	0.0193
	3	23.9848	0.8964	20.5321	0.0194
	4	18.4062	0.9409	22.8315	0.0203
	5	14.8616	0.9632	24.6895	0.0207
ATRIH_Otsu	2	18.4194	0.9484	22.8253	0.0187
	3	14.9975	0.9663	24.6104	0.0190
	4	13.2616	0.9738	25.6789	0.0200
	5	13.5099	0.9735	25.5177	0.0198

Table 9 Comparison of slice 80 brain image segmentation performance by different methods

Algorithms	M	RMSE	SSIM	PSNR	ME
ECS_Otsu	2	44.3625	0.6126	15.1905	0.0424
	3	31.9770	0.8105	18.0340	0.0483
	4	27.1103	0.8567	19.4681	0.0719
	5	25.0474	0.8830	20.1555	0.0845
EGG_Otsu	2	35.0758	0.7230	17.2307	0.0305
	3	30.0227	0.8134	18.5818	0.0371
	4	24.9612	0.8823	20.1855	0.0406
	5	21.9893	0.9103	21.2866	0.0548
NLM2D_Rényi	2	33.4222	0.7532	17.6501	0.0241
	3	28.1949	0.8383	19.1274	0.0296
	4	24.7507	0.8882	20.2590	0.0353
	5	21.1298	0.9177	21.6329	0.0420
TRIH_Otsu	2	30.8797	0.7916	18.3373	0.0216
	3	22.6889	0.8963	21.0145	0.0251
	4	19.2865	0.9278	22.4257	0.0262
	5	16.4322	0.9499	23.8169	0.0269
ATRIH_Otsu	2	18.1404	0.9441	22.9579	0.0200
	3	15.6530	0.9591	24.2389	0.0223
	4	13.9822	0.9675	25.2193	0.0235
	5	12.4933	0.9743	26.1973	0.0238

better and better with the increase of threshold number. This multi-level thresholding segmentation experiment verified the superiority of ATRIH_Otsu once again, and the method can be applied to brain MR image segmentation.

5 Conclusion

The trapezoid region intercept histogram based Otsu method needs to improve the anti-noise capability and detail retention, it is difficult to apply to images with different noise. In this paper, by analyzing the advantages and disadvantages of trapezoid region intercept histogram based Otsu method, an adaptive trapezoid region intercept histogram based Otsu method is proposed. This method is based on 2D histogram of gray value-adaptive weighted neighborhood gray mean, so that the algorithm can give consideration to anti-noise capability and detail retention. In the trapezoid region corresponding to the macro-threshold T_1 of trapezoid region intercept histogram based Otsu method, the hierarchical threshold method was used to further determine the micro-threshold T_2, so as to improve the accuracy of image segmentation. According to the neighborhood of the pixel, the parameter l is calculated adaptively and the noise is corrected according to this adaptive l, so as to enhance the universality of the algorithm. Experimental results show that the three improvement strategies can improve the

algorithm's anti-noise capability or detail retention to some extent. Compared with several mainstream Otsu methods, the adaptive trapezoid region intercept histogram based Otsu method can better segment the images with different noise, showing good universality and anti-noise stability. The quantitative comparison experiments of multi-level thresholding segmentation show that adaptive trapezoid region intercept histogram based Otsu method has good segmentation performance and can be applied to brain MR image segmentation. Although this method can segment image with various noise effectively, the problem of noise identification is a difficult problem at present. So, there is still some noise in the segmentation results. Therefore, improving the performance of the noise recognition method is of great significance to the improvement of this method. And the work of this paper can provide a method reference for the processing of clinical medical images and show good theoretical significance and practical value.

Acknowledgements This work was supported by Hunan Provincial Natural Science Foundation (No. 2020JJ4587), Guangdong Basic and Applied Basic Research Foundation (No. 2019A1515110423), and the Degree and Postgraduate Education Reform Project of Hunan Province (No. 2019JGYB115).

References

Adel K, Khaled A, Ferhat Z (2018) Fully automated brain tumour segmentation system in 3D-MRI using symmetry analysis of brain and level sets. IET Image Process 12(11):1964–1971

Allioui H, Sadgal M, Elfazziki A (2021) Optimized control for medical image segmentation: improved multi-agent systems agreements using Particle Swarm Optimization. J Ambient Intell Human Comput. https://doi.org/10.1007/s12652-020-02682-9

Bahar K, Mehran Y (2018) A new optimized thresholding method using ant colony algorithm for MR brain image segmentation. J Digit Imaging 32(1):162–174

Brain Web [Online] (2020). http://www.med.harvard.edu/AANLIB/. Accessed 16 May 2020

Buvanesvari VK, Suganthi M (2020) Three dimensional modelling of MRI knee images using improved edge detection and finite element modelling. Multimed Tools Appl 79:17045–17056

Castiglione A, Santis AD, Pizzolante R, Castiglione A, Loia V, Palmieri F (2015) On the protection of fMRI images in multi-domain environments. In: Proceedings of 2015 IEEE 29th international conference on advanced information networking and applications, IEEE, pp 476–481.

Castiglione A, Pizzolante R, Palmieri F, Masucci B, Carpentieri B, Santis AD, Castiglione A (2017) On-board format-independent security of functional magnetic resonance images. ACM Trans Embed Comput Syst 16(2):1–15

Ding S, Qu S, Xi Y, Wan S (2020) Stimulus-driven and concept-driven analysis for image caption generation. Neurocomputing 398:520–530

Fan JL, Zhao F (2007) Two-dimensional Otsu's curve thresholding segmentation method for gray-level images. Acta Electron Sin 35(4):751–755

Gao Z, Li Y, Wan S (2020) Exploring deep learning for view-based 3D model retrieval. ACM Trans Multimed Comput Commun Appl 16(1):18–37

He ZY, Sun LN, Huang WG, Chen LG (2012) Thresholding segmentation algorithm based on Otsu criterion and line intercept histogram. Opt Precis Eng 20(10):2315–2323

Himanshu M, Mukesh S (2018) An optimum multi-level image thresholding segmentation using non-local means 2D histogram and exponential Kbest gravitational search algorithm. Eng Appl Artif Intell 71:226–235

Javed A, Kim YC, Khoo MCK, Ward SLD, Nayak KS (2016) Dynamic 3-D MR visualization and detection of upper airway obstruction during sleep using region-growing segmentation. IEEE Trans Biomed Eng 63(2):431–437

Krishnakumar S, Manivannan K (2020) Effective segmentation and classification of brain tumor using rough K means algorithm and multi kernel SVM in MR images. J Ambient Intell Humaniz Comput. https://doi.org/10.1007/s12652-020-02300-8

Li Q, Tang H, Chi JN, Xing XY, Li HT (2017) Gesture segmentation with improved maximum between-cluster variance algorithm. Acta Autom Sin 43(4):528–537

Liu JZ, Li WQ (1993) Automatic thresholding using the Otsu algorithm based on the two-dimensional gray image. Acta Autom Sin 19(1):101–105

Ma JF, Liu Y, Qin X, Gao S (2014) A cell segmentation method based on pseudo median bilateral filtering and level set function. J Nat Sci Beijing Norm Univ 1:41–43

Magudeeswaran V, Bharath S (2020) Brain tissue segmentation for medical decision support systems. J Ambient Intell Humaniz Comput. https://doi.org/10.1007/s12652-020-02257-8

Nie FY, Wang YL, Pan MS, Peng GH, Zhang PF (2013) Two-dimensional extension of variance-based thresholding for image segmentation. Multidimens Syst Signal Process 24(3):485–501

Nie D, Wang L, Ehsan A, Lao CJ, Lin WL, Shen DG (2018) 3-D fully convolutional networks for multimodal isointense infant brain image segmentation. IEEE T Cybern 49(3):1123–1136

Nobuyuki O (1979) A threshold selection method from gray-level histogram. IEEE Trans Syst Man 9(1):62–66

Rutuparna P, Sanjay A, Leena S, Ajith A (2017) An evolutionary gray gradient algorithm for multilevel thresholding of brain MR images using soft computing techniques. Appl Soft Comput 50:94–108

Sankar SP, George DE (2020) Regression neural network segmentation approach with LIDC-IDRI for lung lesion. J Ambient Intell Human Comput. https://doi.org/10.1007/s12652-020-02069-w

Sha CS, Hou J, Cui HX (2016) A robust 2D Otsu's thresholding method in image segmentation. J Vis Commun Image Represent 41:339–351

Shilpa S, Shyam L (2016) An efficient cuckoo search algorithm based multilevel thresholding for segmentation of satellite images using different objective functions. Expert Syst Appl 58:184–209

Song YT, Ji ZX, Sun QS (2014) Brain MR image segmentation algorithm based on markov random field with image patch. Acta Autom Sin 40(8):1754–1763

Tomasi C, Manduchi R (1998) Bilateral filtering for gray and color images. In: Proceedings of the sixth international conference on computer vision, IEEE, pp 839–846

Tongbram S, Shimray BA, Singh LS, Nameirakpam D (2021) A novel image segmentation approach using fcm and whale optimization algorithm. J Ambient Intell Human Comput. https://doi.org/10.1007/s12652-020-02762-w

Wan S, Xia Y, Qi L, Yang YH (2020) Automated colorization of a grayscale image with seed points propagation. IEEE Trans Multimedia 22(7):1756–1768

Wu YQ, Pan Z, Wu WY (2008) Image thresholding based on two-dimensional histogram oblique segmentation and its fast recurring algorithm. J Commun 29(4):77–83

Xiao LY, Ouyang HL, Fan CD (2019) An improved Otsu method for threshold segmentation based on set mapping and trapezoid region intercept histogram. Optik 196:163106

Xiao LY, Ouyang HL, Fan CD, Umer T, Poonia RC, Wan SH (2020) Gesture image segmentation with Otsu's method based on noise adaptive angle threshold. Multimed Tools Appl 79(47–48):35619–35640

Zhang XM, Sun YJ, Zheng YB (2011) Precise two-dimensional Otsu's image segmentation and its fast recursive realization. Acta Electron Sin 39(8):1778–1784

Zhao F, Fan JL, Liu HQ, Lan R, Chen CW (2019) Noise robust multiobjective evolutionary clustering image segmentation motivated by the intuitionistic fuzzy information. IEEE Trans Fuzzy Syst 27(2):387–401